Joint Analog and Passive Beamforming Design for IRS-Aided Secure Cognitive NOMA Systems

Jifa Zhang[†], Wei Wang[†], Jie Tang[§], Nan Zhao[†], Kai-Kit Wong[⋆], Xianbin Wang[‡]

[†]School of Information and Communication Engineering, Dalian University of Technology, Dalian, P. R. China
[§]Department of Electronic Engineering and Information Science, University of Science and Technology of China
[⋆]Department of Electronic and Electrical Engineering, University College London, London WC1E 6BT, U.K.
[‡]Department of Electrical and Computer Engineering, Western University, London, ON N6A 5B9, Canada

Abstract—Due to the ability of channel reconfiguration, intelligent reflecting surface (IRS) can be used to boost the secrecy rate of cognitive non-orthogonal multiple access (NOMA) systems. However, the cost and hardware complexity of full-digital beamforming in existing related studies is high, especially for the systems with massive antennas. In this paper, we investigate the secure transmission for IRS-aided cognitive NOMA systems with cost-effective analog beamforming. The secrecy rate of primary user is maximized subject to the quality of service constraint of secondary user via joint analog and passive beamforming optimization. Owing to the non-convexity, we first transform the problem into two subproblems. Then, each subproblem is tackled via the penalty-based algorithm and the successive convex approximation. Simulation results demonstrate that the proposed transmission scheme has higher energy efficiency and can boost the security of IRS-aided cognitive NOMA systems.

Index Terms—Analog beamforming, cognitive radio, IRS, NOMA, physical layer security.

I. Introduction

Intelligent reflecting surface (IRS), as a promising technique, can boost the performance of wireless communications via reconfiguring wireless channels intelligently [1]. Specifically, IRS is made up of enormous reflection elements integrated on a plane, and passive beamforming can be performed via coordinating the phase shift at each reflection element. In addition, IRS can outperform the conventional active relays in hardware complexity, energy consumption and cost. Owing to the enhanced capacity of desired channels through reconfiguration, IRS can boost the security of wireless communications [2], [3]. Pang *et al.* in [2] studied the secure transmission for IRS-aided unmanned aerial vehicle systems. Yu *et al.* in [3] proposed a robust transmission scheme to guarantee the security of IRS-aided wireless communications with the imperfect wiretap channel state information (CSI).

With the growing number of wireless devices, orthogonal multiple access (OMA) can not satisfy the increasing demand for wireless connections because of limited radio resources. Non-orthogonal multiple access (NOMA) can outperform the conventional OMA in spectrum efficiency via sharing the same resource among all users [4]. For instance, the signals for all power-domain NOMA users are superposed at the transmitter, and then transmitted over a single resource.

Then, successive interference cancellation (SIC) is adopted by each user to decode its own signal [5]. To guarantee proper operation of power-domain NOMA, user with weaker channel gain is allocated with more transmit power, which makes it more vulnerable to eavesdropping. Owing to its capability of channel reconfiguration and enhancement, IRS can be integrated with NOMA to further improve the security and spectrum efficiency [6], [7]. In [6], Zhang *et al.* proposed a robust transmission scheme to guarantee the security of IRS-aided NOMA systems with the imperfect eavesdropping CSI. Unknowing the eavesdropping CSI, Wang *et al.* in [7] proposed a transmission scheme to guarantee the security of IRS-aided NOMA systems. Tang *et al.* in [8] investigated the secrecy performance of IRS-aided NOMA systems.

All the above works assume that the BS adopts the full-digital beamforming, where each antenna is connected to a power-hungry radio frequency (RF) chain. Although full-digital beamforming has better performance, it is not cost-effective to deploy full-digital beamforming in the systems with massive antennas because of high hardware complexity and power consumption [9]. By contrast, the hybrid beamforming (HBF) and analog beamforming consist of lots of low-cost phase shifters and much fewer RF chains. Therefore, HBF and analog beamforming have the advantages of low hardware complexity, low power consumption and easy deployment, which are more suitable for the deployment of massive antennas. Hong *et al.* in [10] maximized the achievable rate of IRS-aided systems with HBF via joint HBF and passive beamforming optimization.

To our knowledge, the secure transmission for IRS-aided cognitive NOMA systems with analog beamforming has not been well investigated. In this paper, we investigate the secure transmission for IRS-aided cognitive NOMA systems with analog beamforming. The secrecy rate of primary user (PU) is maximized subject to the quality of service constraint (QoS) of secondary user (SU) via joint analog and passive beamforming optimization. To address this non-convex problem, we first transform it into two subproblems, and then solve each subproblem via the proposed iterative algorithm.

II. System Model and Problem Formulation

In this section, we first introduce the system model, and then formulate the secrecy rate maximization problem.
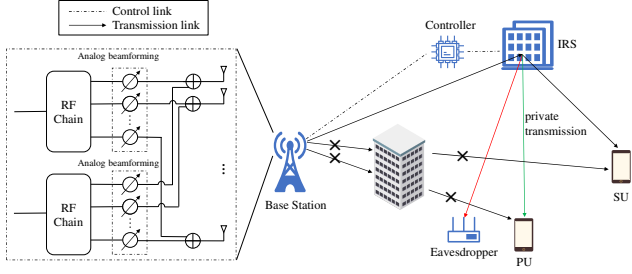
Fig. 1. IRS-aided secure cognitive NOMA systems with analog beamforming.

A. System Model

We consider an IRS-aided secure cognitive NOMA system consisting of a base station (BS) with N_t antennas, a single-antenna cell-center PU, a single-antenna cell-edge SU, an IRS with M reflection elements and an eavesdropper with N_e antennas, as depicted in Fig. 1. Moreover, the BS adopts the analog beamforming to reduce the power consumption and hardware complexity. The eavesdropper aims at obtaining the confidential information from BS to PU. Owing to that the direct links from BS to the users are blocked, an IRS is employed to assist the wireless transmission and enhance the security. The channels from BS to IRS, IRS to PU, IRS to SU and IRS to eavesdropper are represented by $\mathbf{H}_{ai} \in \mathbb{C}^{M \times N_t}$, $\mathbf{h}_1 \in \mathbb{C}^{M \times 1}$, $\mathbf{h}_2 \in \mathbb{C}^{M \times 1}$ and $\mathbf{H}_{ie} \in \mathbb{C}^{N_e \times M}$, respectively. Let $\mathbf{\Phi} = \text{diag}(\mathbf{v}) \in \mathbb{C}^{M \times M}$ stand for the phase shifts of the IRS, where $\mathbf{v}(i) = e^{j\theta_i}$ represents the phase shift of ith reflection element.

Different from existing works, the BS adopts the analog beamforming. Thus, the transmitted signal from the BS can be formulated as

$$\mathbf{x} = \mathbf{f}_1 s_1 + \mathbf{f}_2 s_2, \tag{1}$$

where $s_1 \sim \mathcal{CN}(0,1)$ and $s_2 \sim \mathcal{CN}(0,1)$ are the normalized information symbols of PU and SU, respectively, and $\mathbf{f}_1$ and $\mathbf{f}_2$ are the corresponding analog beamforming vectors.

Therefore, the signal received by PU can be formulated as

$$y_1 = \mathbf{h}_1^H \mathbf{\Phi} \mathbf{H}_{ai} \mathbf{x} + n_1, \tag{2}$$

where $n_1 \sim \mathcal{CN}(0, \sigma_1^2)$ stands for the additive white Gaussian noise (AWGN) at the PU.

The signal received by SU can be expressed as

$$y_2 = \mathbf{h}_2^H \mathbf{\Phi} \mathbf{H}_{ai} \mathbf{x} + n_2, \tag{3}$$

where $n_2 \sim \mathcal{CN}(0, \sigma_2^2)$ denotes the AWGN at the SU.

Similarly, the signal received by the eavesdropper can be expressed as

$$\mathbf{y}_e = \mathbf{H}_{ie} \mathbf{\Phi} \mathbf{H}_{ai} \mathbf{x} + \mathbf{n}_e, \tag{4}$$

where $\mathbf{n}_e \sim \mathcal{CN}(\mathbf{0}, \sigma_e^2 \mathbf{I})$ denotes the AWGN vector at the eavesdropper.

Owing to that the PU is near the IRS, while the SU is far away from it, the channel gains of PU and SU satisfy $\|\mathbf{h}_1\|^2 > \|\mathbf{h}_2\|^2 > 0$. According to the power-domain NOMA

[5], each user first detects the SU's signal via treating the PU's signal as noise. Then, the PU can decode its own signal via removing the detected SU's signal from the received signal. Consequently, the achievable rate of SU and PU at the PU can be given by

$$R_{1,2} = \log_2\left(1 + \frac{\gamma_1 |\mathbf{h}_1^H \mathbf{\Phi} \mathbf{H}_{ai} \mathbf{f}_2|^2}{\gamma_1 |\mathbf{h}_1^H \mathbf{\Phi} \mathbf{H}_{ai} \mathbf{f}_1|^2 + 1}\right), \tag{5}$$

$$R_{1,1} = \log_2\left(1 + \gamma_1 |\mathbf{h}_1^H \mathbf{\Phi} \mathbf{H}_{ai} \mathbf{f}_1|^2\right), \tag{6}$$

respectively, where $\gamma_1 = 1/\sigma_1^2$.

The achievable rate of SU at the SU can be given by

$$R_{2,2} = \log_2\left(1 + \frac{\gamma_2 |\mathbf{h}_2^H \mathbf{\Phi} \mathbf{H}_{ai} \mathbf{f}_2|^2}{\gamma_2 |\mathbf{h}_2^H \mathbf{\Phi} \mathbf{H}_{ai} \mathbf{f}_1|^2 + 1}\right), \tag{7}$$

where $\gamma_2 = 1/\sigma_2^2$.

For the eavesdropper, the eavesdropping rate towards the confidential information s_1 can be given by

$$R_e = \log_2\left|\mathbf{I} + \tilde{\mathbf{Q}}_e^{-1} \gamma_e (\mathbf{H}_{ie} \mathbf{\Phi} \mathbf{H}_{ia}) \mathbf{f}_1 \mathbf{f}_1^H (\mathbf{H}_{ie} \mathbf{\Phi} \mathbf{H}_{ia})^H\right|, \tag{8}$$

where $\tilde{\mathbf{Q}}_e = \gamma_e (\mathbf{H}_{ie} \mathbf{\Phi} \mathbf{H}_{ai}) \mathbf{f}_2 \mathbf{f}_2^H (\mathbf{H}_{ie} \mathbf{\Phi} \mathbf{H}_{ai})^H + \mathbf{I}$ and $\gamma_e = 1/\sigma_e^2$.

Therefore, the secrecy rate of PU can be expressed as

$$R_s = \max(R_{1,1} - R_e, 0). \tag{9}$$

B. Problem Formulation

With the perfect CSI, the secrecy rate of PU is maximized subject to the constant modulus constraint, the transmit power constraint, the SIC decoding constraint and the QoS constraint of SU. The optimization problem can be given by

$$\max_{\mathbf{f}_1, \mathbf{f}_2, \mathbf{v}, p_1, p_2} R_s \tag{10a}$$

$$\text{s.t.} \quad |\mathbf{f}_1(i)| = \sqrt{\frac{p_1}{N_t}}, \ i = 1, \cdots, N_t, \tag{10b}$$

$$|\mathbf{f}_2(i)| = \sqrt{\frac{p_2}{N_t}}, \ i = 1, \cdots, N_t, \tag{10c}$$

$$p_1 + p_2 \leq P_{max}, \ p_1 \geq 0, \ p_2 \geq 0, \tag{10d}$$

$$R_{2,2} \geq \zeta, \tag{10e}$$

$$|\mathbf{v}(i)| = 1, \ i = 1, \cdots, M, \tag{10f}$$

$$R_{1,2} \geq R_{2,2}, \tag{10g}$$

$$|\mathbf{h}_k^H \mathbf{\Phi} \mathbf{H}_{ai} \mathbf{f}_2|^2 \geq |\mathbf{h}_k^H \mathbf{\Phi} \mathbf{H}_{ai} \mathbf{f}_1|^2, k = 1, 2, \tag{10h}$$

where (10b) and (10c) stand for the analog beamforming constraints, while $p_1 \geq 0$ and $p_2 \geq 0$ are the transmit power allocated to $\mathbf{f}_1$ and $\mathbf{f}_2$, respectively. (10d) represents the transmit power constraint at BS. (10e) denotes that the achievable rate at SU should be no less than a given threshold $\zeta > 0$. (10f) is the unit-modulus constraint for the IRS. (10g) guarantees the successful SIC at PU. (10h) implicates the SIC decoding order of users. Problem (10) is challenging to address owing to the coupled variables, the non-convex constraints and the non-concave objective function.

III. PROPOSED ITERATIVE ALGORITHM

In this section, an iterative algorithm based on the AO, the penalty-based algorithm and the SCA is developed to address (10). Specifically, we first transform (10) into two subproblems. Then, each subproblem is solved via the penalty-based algorithm and the SCA.

A. $(\mathbf{f}_1, \mathbf{f}_2, p_1, p_2)$ Optimization With Given $\mathbf{v}$

With any given $\mathbf{v}$, we denote $\mathbf{F}_1 = \mathbf{f}_1 \mathbf{f}_1^H$ ($\mathbf{F}_1 \succeq \mathbf{0}, \text{rank}(\mathbf{F}_1) = 1$) and $\mathbf{F}_2 = \mathbf{f}_2 \mathbf{f}_2^H$ ($\mathbf{F}_2 \succeq \mathbf{0}, \text{rank}(\mathbf{F}_2) = 1$), respectively. (10) can be equivalently formulated as

$$\min_{\mathbf{F}_1, \mathbf{F}_2, p_1, p_2} \quad -\tilde{R}_s \tag{11a}$$

$$s.t. \quad \text{diag}(\mathbf{F}_i) = \frac{p_i}{N_t}, \ i = 1, 2, \tag{11b}$$

$$\text{rank}(\mathbf{F}_i) = 1, \ i = 1, 2, \tag{11c}$$

$$\mathbf{F}_i \succeq \mathbf{0}, \ i = 1, 2, \tag{11d}$$

$$p_1 + p_2 \leq P_{max}, \ p_1 \geq 0, \ p_2 \geq 0, \tag{11e}$$

$$\log_2 \left(1 + \frac{\gamma_2 \text{Tr}(\mathbf{M}_2 \mathbf{F}_2)}{\gamma_2 \text{Tr}(\mathbf{M}_2 \mathbf{F}_1) + 1} \right) \geq \zeta, \tag{11f}$$

$$\frac{\gamma_1 \text{Tr}(\mathbf{M}_1 \mathbf{F}_2)}{\gamma_1 \text{Tr}(\mathbf{M}_1 \mathbf{F}_1) + 1} \geq \frac{\gamma_2 \text{Tr}(\mathbf{M}_2 \mathbf{F}_2)}{\gamma_2 \text{Tr}(\mathbf{M}_2 \mathbf{F}_1) + 1}, \tag{11g}$$

$$\text{Tr}(\mathbf{M}_k \mathbf{F}_2) \geq \text{Tr}(\mathbf{M}_k \mathbf{F}_1), k = 1, 2, \tag{11h}$$

where $\mathbf{M}_k = \mathbf{H}_{ai}^H \boldsymbol{\Phi}^H \mathbf{h}_k \mathbf{h}_k^H \boldsymbol{\Phi} \mathbf{H}_{ai}, k = 1, 2$, $\tilde{R}_s$ is formulated as (12) at the top of the next page and $\hat{\mathbf{Q}}_e = \gamma_e (\mathbf{H}_{ie} \boldsymbol{\Phi} \mathbf{H}_{ai}) \mathbf{F}_2 (\mathbf{H}_{ie} \boldsymbol{\Phi} \mathbf{H}_{ai})^H + \mathbf{I}$. The constraints (11b), (11d), (11e) and (11h) are convex, while the other constraints and the objective function are non-convex. To address it, the constraint (11f) is first formulated into an equivalent form as

$$\gamma_2 \text{Tr}(\mathbf{M}_2 \mathbf{F}_2) - (2^\zeta - 1)(\gamma_2 \text{Tr}(\mathbf{M}_2 \mathbf{F}_1) + 1) \geq 0, \tag{13}$$

which is convex with respect to $\mathbf{F}_1$ and $\mathbf{F}_2$.

Via introducing a slack variable $\beta > 0$, the constraint (11g) can be relaxed as

$$\gamma_1 \text{Tr}(\mathbf{M}_1 \mathbf{F}_2) \geq \beta(\gamma_1 \text{Tr}(\mathbf{M}_1 \mathbf{F}_1) + 1), \tag{14a}$$

$$\gamma_2 \text{Tr}(\mathbf{M}_2 \mathbf{F}_2) \leq \beta(\gamma_2 \text{Tr}(\mathbf{M}_2 \mathbf{F}_1) + 1). \tag{14b}$$

It can be seen that the term $\gamma_1 \text{Tr}(\mathbf{M}_1 \mathbf{F}_1) + 1$ in (14a) is positive. According to the arithmetic and geometric mean (AGM) inequality [11], (14a) can be approximated as

$$2\gamma_1 \text{Tr}(\mathbf{M}_1 \mathbf{F}_2) \geq \left(\frac{\gamma_1 \text{Tr}(\mathbf{M}_1 \mathbf{F}_1) + 1}{a} \right)^2 + (\beta a)^2, \tag{15}$$

where the equality holds if and only if $a = \sqrt{(\gamma_1 \text{Tr}(\mathbf{M}_1 \mathbf{F}_1) + 1)/\beta}$.

For the constraint (14b), we introduce a slack variable ν, which satisfies

$$\gamma_2 \text{Tr}(\mathbf{M}_2 \mathbf{F}_2) \overset{(a)}{\leq} \nu^2 \overset{(b)}{\leq} \beta(\gamma_2 \text{Tr}(\mathbf{M}_2 \mathbf{F}_1) + 1). \tag{16}$$

The inequality (a) in (16) can be further approximated as

$$\gamma_2 \text{Tr}(\mathbf{M}_2 \mathbf{F}_2) \leq -\tilde{\nu}^2 + 2\tilde{\nu}\nu. \tag{17}$$

The right-hand side of (17) stands for the first-order Taylor expansion of the quadratic function ν^2 at the reference point $\tilde{\nu}$, which is a lower bound of the quadratic function ν^2.

The inequality (b) in (16) can be equivalently written as

$$\begin{bmatrix} \gamma_2 \text{Tr}(\mathbf{M}_2 \mathbf{F}_1) + 1 & \nu \\ \nu & \beta \end{bmatrix} \succeq \mathbf{0}. \tag{18}$$

For the rank-one constraint (11c), we formulate it into an equivalent form as

$$(11c) \Leftrightarrow \|\mathbf{F}_i\|_* - \|\mathbf{F}_i\|_2 \leq 0, \ i = 1, 2. \tag{19}$$

For any $\mathbf{F} \in \mathbb{H}^{N_t}$, the inequality $\|\mathbf{F}\|_* \geq \|\mathbf{F}\|_2$ holds. The equality in (19) holds if and only if $\text{rank}(\mathbf{F}) = 1$ [12]. The constraint (19) is non-convex and the penalty-based algorithm in [12] is utilized to address it. In particular, we move the constraint (19) into the objective function as a penalty term, which yields the following problem as

$$\min_{\substack{\mathbf{F}_1, \mathbf{F}_2, p_1, \\ p_2, \beta \geq 0, \nu}} -\tilde{R}_s + \frac{1}{2\rho} \sum_{i=1}^{2} (\|\mathbf{F}_i\|_* - \|\mathbf{F}_i\|_2) \tag{20a}$$

$$s.t. \quad (11b), (11d), (11e), (11h), (13), (15), (17), (18), \tag{20b}$$

where $\rho > 0$ stands for the penalty coefficient. All constraints in (20) are convex. As for the non-convex objective function in (20), the SCA is utilized to address it. Specifically, the objective function is first transformed into a difference of convex, i.e., $-\tilde{R}_s = N_1 - D_1$, where

$$N_1 = -\log_2(1 + \gamma_1 \text{Tr}(\mathbf{M}_1 \mathbf{F}_1))$$
$$-\log_2 |\mathbf{I} + \gamma_e \tilde{\mathbf{H}}_e \mathbf{F}_2 \tilde{\mathbf{H}}_e^H| + \sum_{i=1}^{2} \frac{\|\mathbf{F}_i\|_*}{2\rho}, \tag{21a}$$

$$D_1 = -\log_2 |\mathbf{I} + \gamma_e \tilde{\mathbf{H}}_e (\mathbf{F}_1 + \mathbf{F}_2) \tilde{\mathbf{H}}_e^H| + \sum_{i=1}^{2} \frac{\|\mathbf{F}_i\|_2}{2\rho}, \tag{21b}$$

and $\tilde{\mathbf{H}}_e = \mathbf{H}_{ie} \boldsymbol{\Phi} \mathbf{H}_{ai}$. Both N_1 and D_1 are jointly convex with respect to $\mathbf{F}_1$ and $\mathbf{F}_2$. Then, we introduce Lemma 1 to get a convex upper bound of this non-convex objective function.

Lemma 1. Let f_i be a real-valued function of the matrices $\mathbf{Z} \succeq \mathbf{0}$ and $\mathbf{Y} \succeq \mathbf{0}$, $i = 1, 2$, which is jointly convex in regard to $\mathbf{Z}$ and $\mathbf{Y}$. For the function $g \triangleq f_1 - f_2$, its convex upper bound can be expressed as $f_1 - \tilde{f}_2$, where $\tilde{f}_2$ stands for the first-order Taylor expansion of f_2 at the reference point $(\mathbf{Z}_0, \mathbf{Y}_0)$, as

$$\tilde{f}_2 = f_2(\mathbf{Z}_0, \mathbf{Y}_0) + \text{Tr}(\nabla_{\mathbf{Z}}^H f_2(\mathbf{Z}_0, \mathbf{Y}_0)(\mathbf{Z} - \mathbf{Z}_0))$$
$$+ \text{Tr}(\nabla_{\mathbf{Y}}^H f_2(\mathbf{Z}_0, \mathbf{Y}_0)(\mathbf{Y} - \mathbf{Y}_0)). \tag{22}$$

Proof: Owing to that f_2 is jointly convex in regard to $\mathbf{Z}$ and $\mathbf{Y}$, f_2 is lower bounded by $\tilde{f}_2$, i.e., $f_2 \geq \tilde{f}_2$. In addition, $\tilde{f}_2$ is an affine function in regard to $\mathbf{Z}$ and $\mathbf{Y}$. Thus, we have

$$f_1 - f_2 \leq f_1 - \tilde{f}_2, \tag{23}$$

and $f_1 - \tilde{f}_2$ is jointly convex with regard to $\mathbf{Z}$ and $\mathbf{Y}$. ∎

According to Lemma 1, the objective function in (20) can be replaced with its convex upper bound at the reference point

$$\tilde{R}_s = \log_2\left(1 + \gamma_1 \text{Tr}(\mathbf{M}_1 \mathbf{F}_1)\right) - \log_2\left|\mathbf{I} + \hat{\mathbf{Q}}_e^{-1}\gamma_e(\mathbf{H}_{ie}\boldsymbol{\Phi}\mathbf{H}_{ia})\mathbf{F}_1(\mathbf{H}_{ie}\boldsymbol{\Phi}\mathbf{H}_{ia})^H\right|. \tag{12}$$

$(\mathbf{F}_1^n, \mathbf{F}_2^n)$, which yields the problem as

$$\min_{\substack{\mathbf{F}_1, \mathbf{F}_2, p_1, \\ p_2, \beta \geq 0, \nu}} N_1 - \text{Tr}(\nabla_{\mathbf{F}_1}^H D_1(\mathbf{F}_1^n, \mathbf{F}_2^n)(\mathbf{F}_1 - \mathbf{F}_1^n)) - $$

$$\text{Tr}(\nabla_{\mathbf{F}_2}^H D_1(\mathbf{F}_1^n, \mathbf{F}_2^n)(\mathbf{F}_2 - \mathbf{F}_2^n)) - D_1(\mathbf{F}_1^n, \mathbf{F}_2^n) \tag{24a}$$

$$s.t. \quad (11b), (11d), (11e), (11h), (13), (15), (17), (18), \tag{24b}$$

where $\nabla_{\mathbf{F}_i} D_1$ can be formulated as

$$\nabla_{\mathbf{F}_i} D_1 = \frac{1}{2\rho}\boldsymbol{\lambda}_{max}(\mathbf{F}_i)\boldsymbol{\lambda}_{max}^H(\mathbf{F}_i) - $$

$$\frac{\tilde{\mathbf{H}}_e^H\left(\mathbf{I} + \gamma_e \tilde{\mathbf{H}}_e(\mathbf{F}_1 + \mathbf{F}_2)\tilde{\mathbf{H}}_e^H\right)^{-1}\tilde{\mathbf{H}}_e}{\ln 2}, i = 1, 2. \tag{25}$$

Therefore, (11) is converted to a convex one (24), which can be solved via CVX. According to [3], a rank-one solution $(\bar{\mathbf{F}}_1, \bar{\mathbf{F}}_2)$ can be obtained via solving (24) with sufficiently small ρ. Then, the optimal solution $\bar{\mathbf{f}}_i$ can be recovered from $\bar{\mathbf{F}}_i$ via the eigen-decomposition, $i = 1, 2$.

The penalty-based algorithm for (24) is summarized in Algorithm 1. Through iteratively solving (24) in Step 3, the optimal value of (24) tends to that of (20). According to [12], the sequence $\{\bar{\mathbf{F}}_1^n, \bar{\mathbf{F}}_2^n\}_{n \in \mathbb{N}}$ converges to a stationary point of (20) in polynomial time.

Algorithm 1 Penalty-Based Algorithm for (24)

1: Initialization: Given an initial point $(\bar{\mathbf{F}}_1^0, \bar{\mathbf{F}}_2^0)$, and set the index of iteration $n = 0$ and the convergence tolerance ϱ.
2: **Repeat**
3: With the given $(\bar{\mathbf{F}}_1^n, \bar{\mathbf{F}}_2^n)$, obtain $(\bar{\mathbf{F}}_1^{n+1}, \bar{\mathbf{F}}_2^{n+1})$ via solving (24).
4: $n = n + 1$.
5: **Until** $1 - \frac{\lambda_{max}(\bar{\mathbf{F}}_1^{n+1})}{p_1^{n+1}} \leq \varrho$ and $1 - \frac{\lambda_{max}(\bar{\mathbf{F}}_2^{n+1})}{p_2^{n+1}} \leq \varrho$.
6: Output: $(\bar{\mathbf{F}}_1^{n+1}, \bar{\mathbf{F}}_2^{n+1})$.

B. $\mathbf{v}$ Optimization With Given $(\mathbf{f}_1, \mathbf{f}_2, p_1, p_2)$

With any given $(\mathbf{f}_1, \mathbf{f}_2, p_1, p_2)$, we denote $\mathbf{V} = \mathbf{v}\mathbf{v}^H$ $(\text{rank}(\mathbf{V}) = 1, \mathbf{V} \succeq \mathbf{0})$. Therefore, (10) can be equivalently formulated as

$$\min_{\mathbf{V}} \quad -\check{R}_s \tag{26a}$$

$$s.t. \quad \mathbf{V} \succeq \mathbf{0}, \ \text{diag}(\mathbf{V}) = 1, \tag{26b}$$

$$\text{rank}(\mathbf{V}) = 1, \tag{26c}$$

$$\log_2\left(1 + \frac{\gamma_2 \text{Tr}(\hat{\mathbf{f}}_{22}\hat{\mathbf{f}}_{22}^H\mathbf{V}^T)}{\gamma_2 \text{Tr}(\hat{\mathbf{f}}_{21}\hat{\mathbf{f}}_{21}^H\mathbf{V}^T) + 1}\right) \geq \zeta, \tag{26d}$$

$$\frac{\gamma_1 \text{Tr}(\hat{\mathbf{f}}_{12}\hat{\mathbf{f}}_{12}^H\mathbf{V}^T)}{\gamma_1 \text{Tr}(\hat{\mathbf{f}}_{11}\hat{\mathbf{f}}_{11}^H\mathbf{V}^T) + 1} \geq \frac{\gamma_2 \text{Tr}(\hat{\mathbf{f}}_{22}\hat{\mathbf{f}}_{22}^H\mathbf{V}^T)}{\gamma_2 \text{Tr}(\hat{\mathbf{f}}_{21}\hat{\mathbf{f}}_{21}^H\mathbf{V}^T) + 1}, \tag{26e}$$

$$\text{Tr}(\hat{\mathbf{f}}_{k2}\hat{\mathbf{f}}_{k2}^H\mathbf{V}^T) \geq \text{Tr}(\hat{\mathbf{f}}_{k1}\hat{\mathbf{f}}_{k1}^H\mathbf{V}^T), k = 1, 2, \tag{26f}$$

where $\hat{\mathbf{f}}_{mn} = \text{diag}(\mathbf{h}_m^H)\mathbf{H}_{ai}\mathbf{f}_n, n = 1, 2, m = 1, 2, \bar{\mathbf{h}}_k = \mathbf{H}_{ai}\mathbf{f}_k, k = 1, 2, \bar{\mathbf{Q}}_e = \mathbf{I} + \gamma_e \mathbf{H}_{ie}\text{diag}(\bar{\mathbf{h}}_2)\mathbf{V}\text{diag}(\bar{\mathbf{h}}_2^H)\mathbf{H}_{ie}^H$, and $\check{R}_s$ is given by (27) at the top of next page. The objective function and all the constraints except (26b) and (26f) are non-convex. To address this non-convex problem, we first write the non-convex constraint (26d) into an equivalent form as

$$\gamma_2 \text{Tr}(\hat{\mathbf{f}}_{22}\hat{\mathbf{f}}_{22}^H\mathbf{V}^T) - (2^\zeta - 1)(\gamma_2 \text{Tr}(\hat{\mathbf{f}}_{21}\hat{\mathbf{f}}_{21}^H\mathbf{V}^T) + 1) \geq 0, \tag{28}$$

which is convex with respect to $\mathbf{V}$.

Recalling (15)-(18), the constraint (26e) can be rewritten as

$$2\gamma_1 \text{Tr}(\hat{\mathbf{f}}_{12}\hat{\mathbf{f}}_{12}^H\mathbf{V}^T) \geq \left(\frac{\gamma_1 \text{Tr}(\hat{\mathbf{f}}_{11}\hat{\mathbf{f}}_{11}^H\mathbf{V}^T) + 1}{a}\right)^2 + (\beta a)^2, \tag{29a}$$

$$\gamma_2 \text{Tr}(\hat{\mathbf{f}}_{22}\hat{\mathbf{f}}_{22}^H\mathbf{V}^T) \leq -\tilde{\nu}^2 + 2\tilde{\nu}\nu, \tag{29b}$$

$$\begin{bmatrix} \gamma_2 \text{Tr}(\hat{\mathbf{f}}_{21}\hat{\mathbf{f}}_{21}^H\mathbf{V}^T) + 1 & \nu \\ \nu & \beta \end{bmatrix} \succeq \mathbf{0}. \tag{29c}$$

Therefore, the penalized version of (26) can be given by

$$\min_{\mathbf{V}, \beta \geq 0, \nu} \quad -\check{R}_s + \frac{1}{2\rho}(\|\mathbf{V}\|_* - \|\mathbf{V}\|_2) \tag{30a}$$

$$s.t. \quad (26b), (26f), (28), (29). \tag{30b}$$

All constraints of (30) are convex. For the non-convex objective function in (30), we first rewrite it into a difference of convex as

$$-\check{R}_s + \frac{1}{2\rho}(\|\mathbf{V}\|_* - \|\mathbf{V}\|_2) = \bar{N}_1 - \bar{D}_1, \tag{31}$$

where

$$\bar{N}_1 = -\log_2\left(1 + \gamma_1 \text{Tr}(\hat{\mathbf{f}}_{11}\hat{\mathbf{f}}_{11}^H\mathbf{V}^T)\right) + \frac{\|\mathbf{V}\|_*}{2\rho}$$

$$- \log_2\left|\mathbf{I} + \gamma_e \mathbf{H}_{ie}\text{diag}(\bar{\mathbf{h}}_2)\mathbf{V}\text{diag}(\bar{\mathbf{h}}_2^H)\mathbf{H}_{ie}^H\right|, \tag{32a}$$

$$\bar{D}_1 = -\log_2\left|\mathbf{I} + \sum_{k=1}^2 \gamma_e \mathbf{H}_{ie}\text{diag}(\bar{\mathbf{h}}_k)\mathbf{V}\text{diag}(\bar{\mathbf{h}}_k^H)\mathbf{H}_{ie}^H\right|$$

$$+ \frac{\|\mathbf{V}\|_2}{2\rho}. \tag{32b}$$

Both $\bar{N}_1$ and $\bar{D}_1$ are convex with respect to $\mathbf{V}$. According to Lemma 1, the objective function in (30) can be replaced with its convex upper bound at the reference point $\mathbf{V}^n$, which yields the following problem as

$$\min_{\mathbf{V}, \beta \geq 0, \nu} \quad \bar{N}_1 - \bar{D}_1(\mathbf{V}^n) - \text{Tr}(\nabla_{\mathbf{V}}^H \bar{D}_1(\mathbf{V}^n)(\mathbf{V} - \mathbf{V}^n)) \tag{33a}$$

$$s.t. \quad (26b), (26f), (28), (29), \tag{33b}$$

where $\nabla_{\mathbf{V}} \bar{D}_1$ is the gradient of $\bar{D}_1$ with respect to $\mathbf{V}$, which is formulated as (34) at the top of next page and $\mathbf{X} = \mathbf{I} + \sum_{k=1}^2 \gamma_e \mathbf{H}_{ie}\text{diag}(\bar{\mathbf{h}}_k)\mathbf{V}\text{diag}(\bar{\mathbf{h}}_k^H)\mathbf{H}_{ie}^H$. Thus, the problem (26) is converted to a convex one (33) and can be solved by CVX.

$$\check{R}_s = \log_2\left(1 + \gamma_1 \mathrm{Tr}(\hat{\mathbf{f}}_{11}\hat{\mathbf{f}}_{11}^H \mathbf{V}^T)\right) - \log_2\left|\mathbf{I} + \bar{\mathbf{Q}}_e^{-1}\gamma_e\mathbf{H}_{ie}\mathrm{diag}(\bar{\mathbf{h}}_1)\mathbf{V}\mathrm{diag}(\bar{\mathbf{h}}_1^H)\mathbf{H}_{ie}^H\right|. \tag{27}$$

$$\nabla_{\mathbf{V}}\bar{D}_1 = -\frac{1}{\ln 2}\left(\sum_{k=1}^{2}\gamma_e\mathrm{diag}(\bar{\mathbf{h}}_k^H)\mathbf{H}_{ie}^H\mathbf{X}^{-1}\mathbf{H}_{ie}\mathrm{diag}(\bar{\mathbf{h}}_k)\right)^H + \frac{1}{2\rho}\boldsymbol{\lambda}_{max}(\mathbf{V})\boldsymbol{\lambda}_{max}^H(\mathbf{V}), \tag{34}$$

C. Algorithm Analysis

In summary, the problem (10) is converted to two convex subproblems (24) and (33), and the proposed AO-based algorithm for (10) is summarized in Algorithm 2, which alternatively tackles the two subproblems and guarantees to converge to a stationary point in polynomial time [13].

Algorithm 2 AO-based Algorithm for (10)

1: Initialization: Given an initial point $(\mathbf{f}_1^0, \mathbf{f}_2^0, p_1^0, p_2^0, \mathbf{v}^0)$, and set the iteration index $n = 0$.
2: **Repeat**
3: With the given $(\mathbf{f}_1^n, \mathbf{f}_2^n, p_1^n, p_2^n, \mathbf{v}^n)$, tackle (24) utilizing Algorithm 1 and update $(\mathbf{F}_1^{n+1}, \mathbf{F}_2^{n+1})$.
4: Decompose $\mathbf{F}_i^{n+1} = \mathbf{f}_i^{n+1}\mathbf{f}_i^{n+1,H}, i = 1, 2$.
5: With the given $(\mathbf{f}_1^{n+1}, \mathbf{f}_2^{n+1}, p_1^{n+1}, p_2^{n+1}, \mathbf{v}^n)$, tackle (33) utilizing Algorithm 1 and update $\mathbf{V}^{n+1}$.
6: Decompose $\mathbf{V}^{n+1} = \mathbf{v}^{n+1}\mathbf{v}^{n+1,H}$.
7: $n = n + 1$.
8: **Until** convergence or reach maximum iteration number.
9: Output: $(\mathbf{f}_1^{n+1}, \mathbf{f}_2^{n+1}, p_1^{n+1}, p_2^{n+1}, \mathbf{v}^{n+1})$.

IV. SIMULATION RESULTS

In this section, we present simulation results to verify the effectiveness of the proposed secure transmission scheme. The BS, IRS, PU, SU and eavesdropper are located at (10, -20, 5), (0, 0, 2), (5, 0, 0), (5, 8, 0) and (7, 7, 0) in meters, respectively. We set $N_t = 4$, $N_e = 2$, $M = 9$ and $\sigma_1^2 = \sigma_2^2 = \sigma_e^2 = -75$ dBm, respectively. All the channels are modeled as Rician fading channel. For instance, the channel from BS to IRS can be given by

$$\mathbf{H}_{ai} = \sqrt{L_0 d_{ai}^{-\alpha_{ai}}}\left(\sqrt{\frac{k_{ai}}{1+k_{ai}}}\mathbf{H}_{ai}^{\mathrm{L}} + \sqrt{\frac{1}{1+k_{ai}}}\mathbf{H}_{ai}^{\mathrm{NL}}\right), \tag{35}$$

where k_{ai} stands for the Rician factor, $L_0 = -30$ dB, α_{ai} is the path-loss exponent and d_{ai} stands for the distance between IRS and BS. $\mathbf{H}_{ai}^{\mathrm{L}}$ and $\mathbf{H}_{ai}^{\mathrm{NL}} \backsim \mathcal{CN}(\mathbf{0}, \mathbf{I})$ represent the line-of-sight (LoS) and non-LoS component, respectively. The path-loss exponent for $\mathbf{H}_{ai}$ is 2, and those for $\mathbf{h}_1$, $\mathbf{h}_2$, and $\mathbf{H}_{ie}$ are 2.8. The Rician factor for all channels is set to 5. ϱ and ς are set to 10^{-3} and 10^{-4}, respectively.

For comparison, we study the following benchmarks. 1) Random Phase: With random phase shifts at IRS, the secrecy rate is maximized via designing the analog beamforming. 2) Full Digital: The BS adopts the full-digital beamforming,

whose performance is a upper bound of the analog beamforming. 3) OMA: The system adopts the frequency division multiple access and the frequency band is equally allocated to the two users. Thus, the achievable rate at each user can be given by

$$R_k^{OMA} = \frac{1}{2}\log_2\left(1 + \frac{2|\mathbf{h}_k^H\boldsymbol{\Phi}\mathbf{H}_{ai}\mathbf{f}_k|^2}{\sigma_k^2}\right), \quad k = 1, 2. \tag{36}$$

Fig. 2 plots the average secrecy rate versus the maximum transmit power P_{max}, with $\zeta = 0.3$ bps/Hz. From Fig. 2, we can conclude that the average secrecy rate increases with P_{max} for all the schemes. This is because that the additional transmit power can improve the SINRs at the users, which increases the secrecy rate. Moreover, the proposed Scheme outperforms "Random Phase" and OMA obviously owing to the higher spectrum efficiency and passive beamforming gain. Moreover, the proposed Scheme slightly underperforms "Full Digital", and the analog beamforming has the advantages of lower hardware complexity and cost. Thus, the proposed analog beamforming scheme is more effective.

In Fig. 3, we depict the average secrecy rate versus the number of reflecting elements, with $(P_{max}, \zeta) = (30\,\mathrm{dBm}, 0.3\,\mathrm{bps/Hz})$. From Fig. 2, we can conclude that the secrecy rate achieved by all the schemes increases with M because additional reflecting elements can improve both the receiving and reflecting beamforming gain of IRS. In addition, the proposed Scheme outperforms "Random Phase" and OMA. Besides, the performance gap between "Full Digital" and the proposed Scheme is very small.

Fig. 4 shows the secrecy energy efficiency (SEE) versus the antenna number at BS, with $(P_{max}, \zeta) = (30\,\mathrm{dBm}, 0.3\,\mathrm{bps/Hz})$. Ignoring the low power consumption of IRS, the SEE can be given by [14]

$$\mathrm{SEE} = \frac{R_s}{P_{max} + N_{rf}P_{rf} + N_{ps}P_{ps} + P_B} \quad (\mathrm{bps/Hz/W}), \tag{37}$$

where $P_B = 0.2$ W stands for the baseband power consumption. N_{rf} and N_{ps} are the number of RF chains and phase shifters, respectively. $P_{rf} = 0.3$ W and $P_{ps} = 0.04$ W represent the power consumed by each RF chain and phase shifter, respectively. For the full-digital beamforming, $N_{rf} = N_t$ and $N_{sp} = 0$, while $N_{rf} = 2$ and $N_{sp} = 2N_t$ for the analog beamforming. As shown in the figure, the proposed Scheme outperforms the other benchmarks in SEE. Moreover, the SEE of "Full Digital" decreases dramatically with N_t owing to the increase of power-hungry RF chains. Thus, the analog beamforming is more suitable than the full-
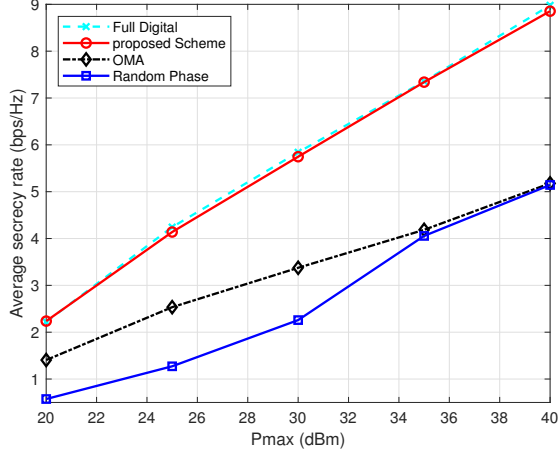
Fig. 2. Average secrecy rate versus the maximum transmit power P_{max}, with $\zeta = 0.3\,\text{bps/Hz}$.
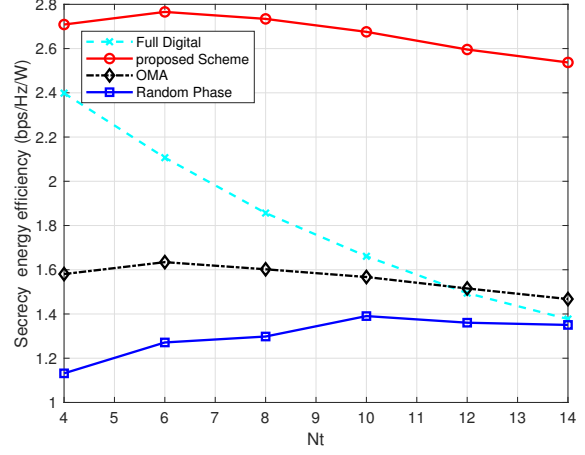

Fig. 4. Secrecy energy efficiency versus the antenna number at the BS, with $(P_{max}, \zeta) = (30\,\text{dBm}, 0.3\,\text{bps/Hz})$.
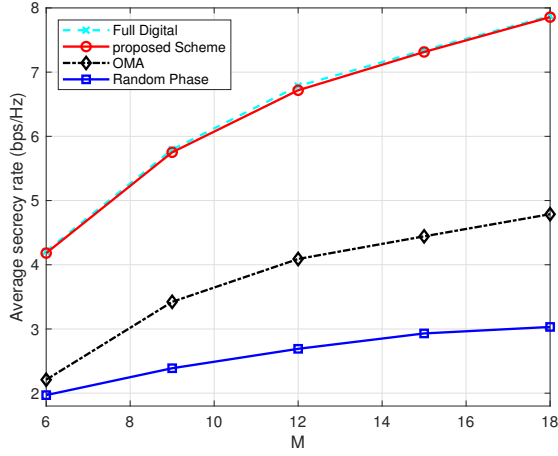

Fig. 3. Average secrecy rate versus the number of reflecting elements, with $(P_{max}, \zeta) = (30\,\text{dBm}, 0.3\,\text{bps/Hz})$.

digital beamforming for the deployment of massive antennas.

V. CONCLUSIONS

In this paper, we deployed an IRS to boost the security of cognitive NOMA systems with cost-effective analog beamforming and a scheme was proposed to guarantee the secure transmission of PU. Specifically, the secrecy rate of PU was maximized subject to the QoS constraint of SU via joint analog and passive beamforming optimization. To address this problem with the non-convex constraints and coupled variables, we first decomposed it into two subproblems, and then solved each subproblem via the penalty-based algorithm and the SCA. The effectiveness of the proposed secure transmission scheme was demonstrated via simulation results.

REFERENCES

[1] Q. Wu and R. Zhang, "Towards smart and reconfigurable environment: Intelligent reflecting surface aided wireless network," *IEEE Commun. Mag*, vol. 58, no. 1, pp. 106–112, Jan. 2020.

[2] X. Pang, N. Zhao, J. Tang, C. Wu, D. Niyato, and K.-K. Wong, "IRS-assisted secure UAV transmission via joint trajectory and beamforming design," *IEEE Trans. Commun.*, vol. 70, no. 2, pp. 1140–1152, Feb. 2022.

[3] X. Yu, D. Xu, Y. Sun, D. W. K. Ng, and R. Schober, "Robust and secure wireless communications via intelligent reflecting surfaces," *IEEE J. Sel. Areas Commun.*, vol. 38, no. 11, pp. 2637–2652, Nov. 2020.

[4] Z. Ding, Y. Liu, J. Choi, Q. Sun, M. Elkashlan, C.-L. I., and H. V. Poor, "Application of non-orthogonal multiple access in LTE and 5G networks," *IEEE Comm. Mag.*, vol. 55, no. 2, pp. 185–191, Feb. 2017.

[5] N. Zhao, W. Wang, J. Wang, Y. Chen, Y. Lin, Z. Ding, and N. C. Beaulieu, "Joint beamforming and jamming optimization for secure transmission in MISO-NOMA networks," *IEEE Trans. Commun.*, vol. 67, no. 3, pp. 2294–2305, Mar. 2019.

[6] Z. Zhang, L. Lv, Q. Wu, H. Deng, and J. Chen, "Robust and secure communications in intelligent reflecting surface assisted NOMA networks," *IEEE Commun. Lett.*, vol. 25, no. 3, pp. 739–743, Mar. 2021.

[7] W. Wang, X. Liu, J. Tang, N. Zhao, Y. Chen, Z. Ding, and X. Wang, "Beamforming and jamming optimization for IRS-aided secure NOMA networks," *IEEE Trans. Wireless Commun.*, vol. 21, no. 3, pp. 1557–1569, Mar. 2022.

[8] Z. Tang, T. Hou, Y. Liu, J. Zhang, and L. Hanzo, "Physical layer security of intelligent reflective surface aided NOMA networks," *IEEE Trans. Veh. Tech.*, vol. 71, no. 7, pp. 7821–7834, Jul. 2022.

[9] S. Han, C.-l. I, Z. Xu, and C. Rowell, "Large-scale antenna systems with hybrid analog and digital beamforming for millimeter wave 5G," *IEEE Comm. Mag.*, vol. 53, no. 1, pp. 186–194, Jan. 2015.

[10] S. H. Hong, J. Park, S.-J. Kim, and J. Choi, "Hybrid beamforming for intelligent reflecting surface aided millimeter wave MIMO systems," *IEEE Trans. Wireless Commun.*, vol. 21, no. 9, pp. 7343–7357, Sep. 2022.

[11] M. Vamanamurthy and M. Vuorinen, "Inequalities for means," *J. Math. Anal. Appl*, vol. 183, no. 1, pp. 155–166, Apr. 1994.

[12] X. Yu, D. Xu, D. W. K. Ng, and R. Schober, "IRS-assisted green communication systems: Provable convergence and robust optimization," *IEEE Trans. Commun.*, vol. 69, no. 9, pp. 6313–6329, Sept. 2021.

[13] M. Razaviyayn, M. Hong, and Z.-Q. T. Luo, "A unified convergence analysis of block successive minimization methods for nonsmooth optimization," *SIAM J. Optim.*, vol. 23, pp. 1126–1153, Jan. 2013.

[14] Z. Xiao, L. Zhu, Z. Gao, D. O. Wu, and X.-G. Xia, "User fairness non-orthogonal multiple access (NOMA) for millimeter-wave communications with analog beamforming," *IEEE Trans. Wireless Commun.*, vol. 18, no. 7, pp. 3411–3423, Jul. 2019.